nanomaterials

MDPI

Article

Ruling factors in cinnamaldehyde hydrogenation: activity and selectivity of Pt-Mo catalysts

Marta Stucchi[1,*], Maela Manzoli[2], Filippo Bossola[3], Alberto Villa[1] and Laura Prati[1]

[1] Chemistry Department, University of Milano, Via C. Golgi 19, 20133 Milano (IT); marta.stucchi@unimi.it; alberto.villa@unimi.it; laura.prati@unimi.it
[2] Department of Drug Science and Technology and NIS Centre for Nanostructured Interfaces and Surfaces, University of Turin, Via P. Giuria 9, 10125 Torino (IT); maela.mazoli@unito.it
[3] Istituto di scienze e tecnologie chimiche "Giulio Natta" (SCITEC) CNR, Via C. Golgi 19, 20133 Milano (IT); filippo.bossola@scitec.cnr.it
* Correspondence: marta.stucchi@unimi.it ; Tel.: +39 0250314364

Abstract: To obtain selective hydrogenation catalysts with low noble metal content, two carbon-supported Mo-Pt bimetallic catalysts have been synthesized from two different molybdenum precursors, i.e. Na_2MoO_4 and $(NH_4)_6Mo_7O_{24}$. The results obtained by X-ray photoelectron spectroscopy (XPS) and transmission electron microscopy (TEM) combined with the presence and strength of acid sites clarified the different catalytic behavior toward cinnamaldehyde hydrogenation. After impregnating the carbon support with Mo precursors, each sample was used, either as it or treated at 400 °C in N_2 flow, as support for Pt nanoparticles (NPs). The heating treatment before Pt deposition had a positive effect on the catalytic performance. Indeed, TEM analyses showed very homogeneously dispersed Pt NPs only when they were deposited on the heat treated Mo/C supports and XPS analyses revealed an increase in both exposure and reduction of Pt, probably tuned by different MoO_3/MoO_2 ratios. Moreover, the different acid properties of the catalysts resulted in different selectivity.

Keywords: molybdenum; cinnamaldehyde; cinnamaldehyde hydrogenation; carbon supported Mo; bimetallic Pt structure; selectivity.

Citation: Lastname, F.; Lastname, F.; Lastname, F. Title. *Nanomaterials* **2021**, *11*, x. https://doi.org/10.3390/xxxxx

Received: date
Accepted: date
Published: date

1. Introduction

The development of green and sustainable processes is directly connected to the discovering of new heterogeneous catalytic systems capable of selectively transforming bio-derived organic molecules [1]. Decisive factors in the development of sustainable chemical processes are efficiency and selectivity. In this context, the catalytic reduction of carbonyl compounds using H_2 is a green method to obtain high-added value alcohols for the production of fine chemicals [2]. Many highly active homogeneous or heterogeneous catalysts based on noble metals have been developed for this purpose [3]. Noble metals such as Ru, Pt and Pd are among the best candidates for catalytic hydrogenation processes [4]. However, they are not the best option considering availability and increasing price. On the other hand, they can be coupled with less precious and active metals, which can improve their performance together with allow to use them in a minor extent. Among non-noble transition metals, molybdenum has already been reported as a possible auxiliary low cost catalyst for hydrogenation. For example, molybdenum carbides have been studied in deep as low cost catalysts for the hydrogenation of levulinic acid to γ-valerolactone [5]. Moreover, Hoang-Van and Zegaoui reported the effects of MoO_3 on the catalytic properties of Pt for the selective hydrogenations of acrolein and allyl alcohol [6], whereas

Wang et al. [7] reported the effect of Mo on the acidity of Pt/TiO_2 catalyst. Mo-based catalysts synthesized by different approaches have been shown to present different activities. This is not a novelty in heterogeneous catalysis, but the reason remains still unclear. Indeed, the different behaviour has been normally explained in terms of different Strong Metal Support Interaction (SMSI) or residual chemicals [8][9].

On the basis of these findings, here we investigated the effect of two different Mo salt precursors in the preparation of Pt-Mo catalysts, that will be tested in the selective hydrogenation of cinnamaldehyde. Hydrogenation of α,β-unsatured aldehydes to the corresponding unsatured alcohols is often studied as a model reaction, considering that the development of selective catalysts for this class of reactions is challenging since the simultaneous presence of the carbon-carbon double bond and the carbonyl group [10]. Cinnamaldehyde (CAL) is the most investigated model compound for discriminating the catalytic selectivity for C=C or C=O hydrogenation. Possible pathways are reported in Fig. 1.

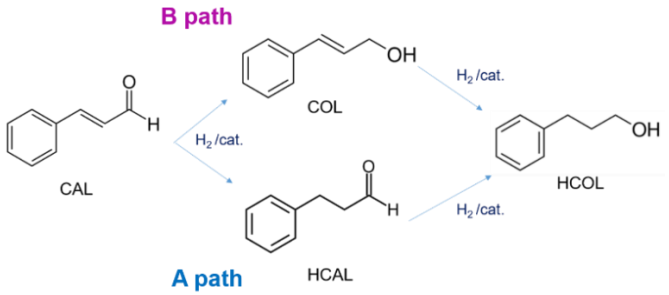

Figure 1. Cinnamaldehyde hydrogenation pathway.

Moreover the reaction presents an industrial interest as both hydrocinnamaldehyde (HCAL) or cinnamyl alcohol (COL) are very important intermediates for the synthesis of many fine chemicals, perfumes and pharmaceuticals [11]. HCAL was found to be essential intermediate in the preparation of a drug used in the treatment of HIV. COL is one of the most used product in perfumery chemicals [12]. On the other hand, also hydrocinnamyl alcohol (HCOL) is desired as it represents an important chemical in pharmaceutical market and cosmetic industry [13]. The strategic importance of this reaction lies on the development of very selective catalysts able to direct the hydrogenation toward the desired product. Ma et al. [14] completely hydrogenated CAL to HCOL by Pt supported on carbon nanotubes (CNTs) with 80 % of selectivity, but only after 12 h of reaction, and in many other cases HCOL is produced but with low selectivity [15]. Considering the selectivity of the process, some researches pointed out a possible role of the metal-support interaction [16] [2], with the charge transfers between the support and the metallic phase that increased the selectivity toward COL, higher with electron-rich active sites [17][18]. However, it was also found that electron-deficient Au NPs show high selectivity to COL in such reaction [19]. Again, other research works report that Lewis acids or metallic promoters are beneficial for enhancing selectivity to COL, because the electropositive metal species on the surface act as electrophilic or Lewis sites for the adsorption and activation of the C=O bond [10].

To be active and selective for cinnamaldehyde hydrogenation, Pt has been also modified with other metals: Mahata et al. [20] reported the effect of Fe and Zn promotion. In that case, the addition of these metals to Pt was found to improve both the activity and the selectivity to COL, due to the creation of new sites for the activation of the aldehydic group. Wang et al. [21] studied the effect of Cu on Pt, proving that Pt-Cu/SiO_2 was more selective toward COL than monometallic Pt/SiO_2, due to the increase in the amount of the Pt^0 on the surface, derived from the interaction between Pt and Cu. To the best of our

knowledge, there are only two recent papers reporting Pt modified by Mo in cinnamaldehyde hydrogenation [22][23]. In the first by Wang et al. [22] SBA-15 was modified with Mo_2N nanoparticles and then used for Pt deposition. A synergistic effect between Pt and Mo_2N was observed, and both activity and selectivity to COL were improved. In the second one [23], Pt was supported on MoO_3 and decorated by FeO_x. The specific acidity of Pt-FeO_x interfaces was shown to be advantageous for the chemisorption and activation of C=O bond, promoting the selective hydrogenation of CAL to COL. In the present paper, we investigated the role of Mo-precursor on the catalytic behaviour of Pt-Mo on carbon catalysts in cinnamaldehyde hydrogenation. We were able to demonstrate that selectivity and activity of Pt-Mo catalysts are strictly connected with their physico-chemical properties, which in turn depended on both Mo precursor and heat treatment. A thermal pretreatment of Mo/C has been shown to be beneficial in terms of activity, but the precursor of Mo appeared to be crucial for the selectivity of the reaction.

2. Materials and Methods

2.1. Catalyst synthesis

Mo supported on carbon was synthesized by wet impregnation. The carbon support was Activated Charcoal Norit from Sigma-Aldrich. Two different catalysts were obtained by varying the Mo precursor, which was Na_2MoO_4 (Sigma Aldrich) or $(NH_4)_6Mo_7O_{24}$ (Sigma Aldrich), respectively. Mo loading was 10 % wt. in both cases. The calculated amount of Mo salt precursor was dissolved in milli-Q water (100 ml/g of carbon). Then, carbon support was added maintaining the solution under stirring. Impregnation lasted 4 h, at room temperature (RT). After 4 h, temperature was increased at 80 °C, until the complete evaporation of the solvent. Half of the powder was used as it to support Pt nanoparticles (NPs) (labelled as fresh sample); the other half was submitted to thermal treatment at 400 °C in N_2 flow (5 ml min^{-1}) and then also used as support for Pt NPs (labelled as 400N sample). Pt NPs have been synthesized using sodium tetrachloroplatinate(II) hydrate (Na_2PtCl_4•3 H_2O) as precursor. A 10 mg ml^{-1} of Na_2PtCl_4 solution was prepared first. 1 ml of the Na_2PtCl_4 solution was diluted in 50 ml of H_2O (milli-Q), and 1 g of the Mo/C powder was then added in the solution under continuous stirring. The amount of Mo/C was calculated to have a final 1 % wt. Pt loading. The solution was kept under continuous stirring at RT for 2 h, to impregnate the Pt^{II} salt on the Mo/C support. The powder was filtered and washed with distilled water, then suspended again in 50 ml of H_2O for the reduction of Pt. The reducing agent was $NaBH_4$ (powder ≥98%, Sigma Aldrich). For such step, $NaBH_4$ was added directly under stirring, calculating the amount to have a $NaBH_4$:metal molar ratio of 8:1. After 1 h, catalysts was filtered, washed, and dried at 80 °C for 2 h. Following the above procedure, four samples were prepared. The description and the corresponding labels are summarized in Table 1.

Table 1. Samples list and description.

n.	Sample	Description
1	Pt-Mo(NH_4)_fresh	Pt NPs on active carbon impregnated with $(NH_4)_6Mo_7O_{24}$.
2	Pt-Mo(NH_4)_400N	Pt NPs on thermally treated (400°C in N_2) active carbon impregnated with $(NH_4)6Mo_7O_{24}$.
3	Pt-Mo(Na)_fresh	Pt NPs on active carbon impregnated with Na_2MoO_4.
4	Pt-Mo(Na)_400N	Pt NPs on thermally treated (400°C in N_2) active carbon impregnated with Na_2MoO_4.

2.2 Characterization methods

Transmission electron microscopy (TEM) characterization of the catalysts was performed by using a side entry JEOL 3010-UHR HRTEM microscope operating at 300 kV, equipped with a LaB_6 filament, with a (2k×2k)-pixel Gatan US1000 CCD camera and with an OXFORD INCA EDS instrument for atomic recognition via energy dispersive spectroscopy (EDS). The powdered samples were deposited on copper grids, coated with a porous carbon film. A statistically representative number of particles (200-300 nanoparticles) was counted in order to obtain the Pt particle size distributions. The mean particle diameter (d_m) was calculated using the following equation:

$$d_m = \Sigma d_i n_i / \Sigma n_i$$

where n_i is the number of particles of diameter d_i.

It is worth noting that as prepared and treated samples were stable to prolonged exposition under the electron beam of the instrument (no metal coalescence, nor modification of the Mo-activated carbon support).

X-ray photoelectron spectra (XPS) were taken in an M-probe apparatus (Surface Science Instruments) for the determination of surface composition and oxidation state of the metals. The source was monochromatic Al K radiation (1486.6 eV). Data reprocessing was performed by Esca Hawk software. The XPS lines of C 1s, O 1s, Mo 4f and Mo 3d regions were recorded.

Ammonia Temperature Programmed Desorption (NH_3-TPD) analyses were performed using an home-made gas feeding apparatus described elsewhere [24] and connected downstream to a mass spectrometer (Hiden Analytical, HPR20). The samples were treated 130 °C under He flow for 1 h. Next, the temperature was lowered to 70 °C and ammonia was adsorbed by pulses of 100 μL until saturation. The samples were then purged at the same temperature with a 20 mL/min He flow. The desorption was performed by ramping up the temperature (8 °C/min) until about 550 °C.

2.3 Catalytic reaction

Cinnamaldehyde hydrogenation has been carried out in a batch autoclave equipped with a glass inlet, at 80 °C and 5 bar of H_2. The amount of the catalyst was calculated in order to have a metal:substrate molar ratio equal to 1:1000. The starting concentration of CAL was 0.15 M in 2-propanol. GC analyses performed by a Thermo Scientific TRACE 1300 Instrument equipped with an Agilent HP-5 column gave CAL conversion and products formation over time, using undecane as an external standard. Sampling occurred at time 0 and every 30 minutes, until the end of the reaction. Quantification of products were performed by calibrating the response with authentic samples.

3. Results and discussion

Four samples (Table 1) consisting of 1%wt. Pt supported on 10%wt. Mo/C synthesized from $(NH_4)_6Mo_7O_{24}$ or Na_2MoO_4 have been prepared and tested in cinnamaldehyde hydrogenation (Table 2).

Table 2. Catalytic results of cinnamaldehyde hydrogenation by Pt-Mo catalysts.

n.	Catalyst	In. activity [a]	Conv. % (6h)[b]	HCAL Sel.%[c]	HCOL Sel.%	COL Sel.%
1	**Pt-Mo(Na)_fresh**	0	0	-	-	-
2	**Pt-Mo(NH_4)_fresh**	0	0	-	-	-
3	**Pt-Mo(Na)_400N**	330.9	66.4	64.3	-	35.7
4	**Pt-Mo(NH_4)_400N**	526.4	50.8	23.6	76.4	-

Reaction conditions: CAL 0.15 M in 2-propanol; 80°C; 5 bar of H2; metal:substrate molar ratio 1000. [a] Initial activity calculated at 30 min of reaction, as moles converted per moles of metal. [b] Conversion calculated after 6h, as % of moles of converted substrate. [c] Selectivity calculated as % of by-products formed.

The carbon was first impregnated with the chosen precursor and then used as support for Pt NPs as it or treated at 400 °C in nitrogen. In the catalytic test the cinnamaldehyde starting concentration was set to 0.15 M in 2-propanol, and the reaction occurred at 80 °C and 5 bar of H_2 with a (Pt) metal:substrate molar ratio 1000. The catalytic results are shown in Table 2. When Pt has been deposited on the fresh Mo/C, the catalysts did not show any activity (Table 2, entries 1 and 2), whereas when it has been deposited on the heat treated Mo/C, the catalysts are active (Table 2, entries 3 and 4). Pt-Mo(Na)_400N achieved 66.4% conversion after 6 hours of reaction, whereas Pt-Mo(NH_4)_400N reached 50.8% (Table 2, entries 3 and 4). However, the initial activity of the Pt-Mo(Na)_400N was lower (330.9 h^{-1}) than that of Pt-Mo(NH_4)_400N (526.4 h^{-1}) (Table 2).

In fact, reaction profiles and selectivity over time (Figs. 2 and 3) showed higher initial activity for Pt-Mo(NH_4)_400N (Table 2 and figure 2), but the conversion reaches a plateau after 3 h of reaction, which could point out a deactivation of the active sites. On the contrary, Pt-Mo(Na)_400N showed a constant increasing CAL conversion over time (Fig. 3) despite the lower initial activity.

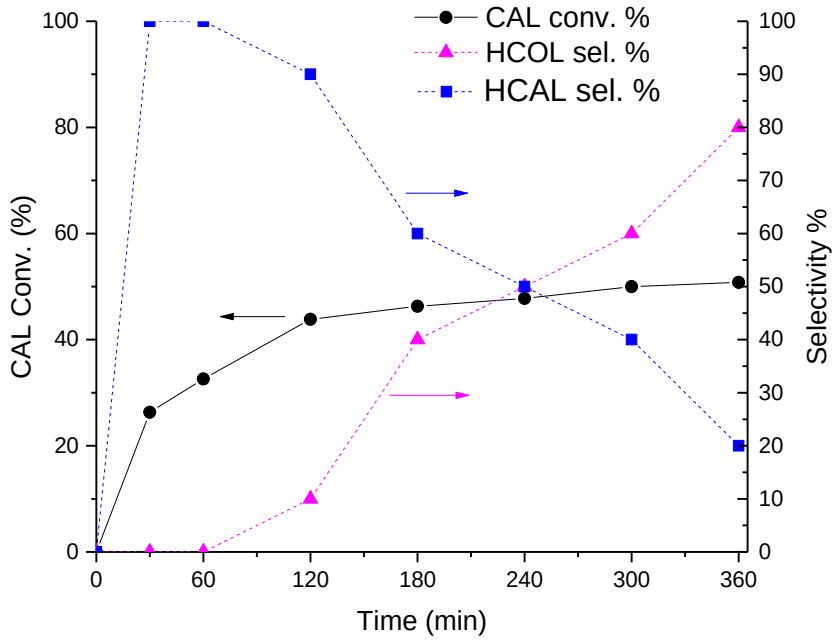

Figure 2. CAL hydrogenation reaction profile vs. time. CAL conversion % (solid line, left Y axis) along with HCAL and HCOL selectivity % (dashed lines, right Y axis) over Pt-Mo(NH_4)_400N.

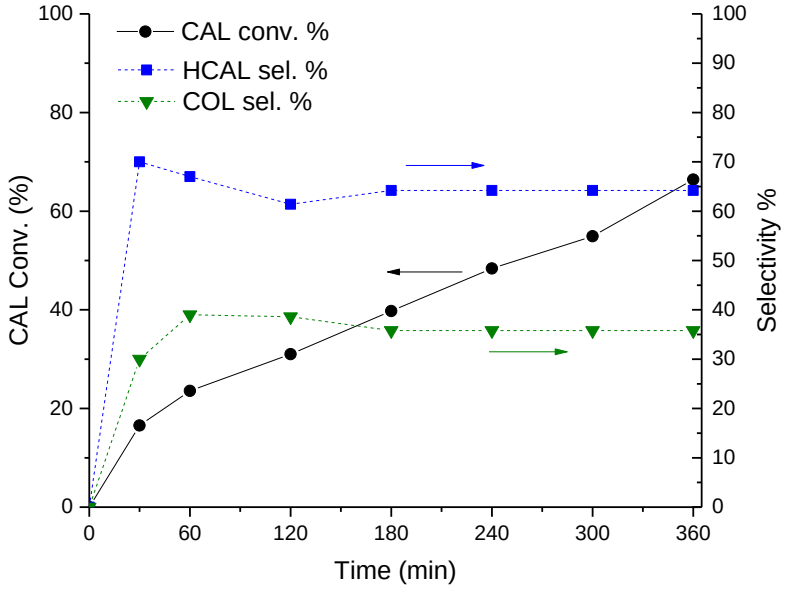

Figure 3. CAL hydrogenation reaction profile vs. time. CAL conversion % (solid line, left Y axis) along with HCAL and COL selectivity % (dashed lines, right Y axis) over Pt-Mo(Na)_400N.

Concerning with selectivity, the Pt-Mo(NH_4)_400N catalyst (Fig. 2) initially converted CAL into HCAL quantitatively, but after 1 hour of reaction (at about 30 % of CAL conversion) HCAL started to be converted to HCOL, which reached a selectivity of 76.4 % at 6 hours of reaction (at 50.8 % of CAL conversion). Differently, in the presence of Pt-Mo(Na)_400N (Fig. 3), COL and HCAL seems to be formed contemporary reaching a steady state, with a selectivity to COL and HCAL around 35 % and 65 %, respectively (see Table 2), regardless the conversion.

Subsequently, we observed that, depending on the Mo precursors, the catalysts showed very different catalytic performance: Pt-Mo(NH_4)_400N presented a very fast hydrogenation of double bond which in turn did not allow to obtain COL. However, the catalyst was also able to hydrogenate the carbonyl group thus producing HCOL from HCAL. On the contrary, Pt-Mo(Na)_400N was able to hydrogenate both group with a more similar rate, thus producing COL+HCAL. However, HCAL is not converted to HCOL meaning that the catalyst was not able to hydrogenate the CHO group if it is not conjugated with the double bond.

Therefore, a detailed characterization has been carried out to explain the huge different catalytic behaviour displayed by the Pt-Mo(Na)_fresh and Pt-Mo(NH4)_fresh catalysts (not active) and the corresponding Pt-Mo(Na)_400N and Pt-Mo(NH4)_400N catalysts (active). Moreover, these studies would be useful to establish structure-activity relationships by comparing Pt-Mo(Na)_400N and Pt-Mo(NH_4)_400N catalysts. The TEM images of the Pt-Mo(Na)_fresh and the corresponding Pt-Mo(Na)_400N are reported in Fig. 4 (a and b).

Only few very rare Pt nanoparticles have been observed in some regions of the sample when Pt has been deposited before the heat treatment (not shown), being both Mo and Pt highly dispersed on the support. EDS analysis revealed very weak peaks related to both Pt and Mo (Figure SI-1, a). However, ICP analysis confirmed the actual loading of 1 %wt. of Pt. A very low signal related to Na was also detected (0.11 wt%). On the contrary, when Pt has been deposited after the heat treatment of Mo/C, highly dispersed Pt nanoparticles

with homogeneous shape and average size equal to 1.2 ± 0.3 nm were observed (Fig. 3, b and c). EDS analyses showed homogeneous distribution of both Pt (1.42 wt%) and Mo (0.30 wt%) (Figure SI-1, b). In this case, a very low amount of Na (0.06 wt %) was found.

TEM-EDS analyses of the Pt-Mo(NH_4)_fresh and Pt-Mo(NH_4)_400N catalysts are reported in Fig. 5. Also in this case, the Pt nanoparticles are not visible in the Pt-Mo(NH_4)_fresh catalyst (Fig. 5a), but both Mo (0.41 wt%) and Pt (0.14 wt%) were detected by the EDS probe. Similarly to what observed for Pt-Mo(Na)_400N, Pt nanoparticles with average size of 2.0 ± 0.5 nm were observed in Pt-Mo(NH_4)_400N (Fig 5, b and c). EDS mapping showed both Mo (1.61 wt%) and Pt (1.59 wt%) homogeneously distributed on the support. In this case, also some big Pt nanoparticle agglomerates were detected (Figure SI-2).

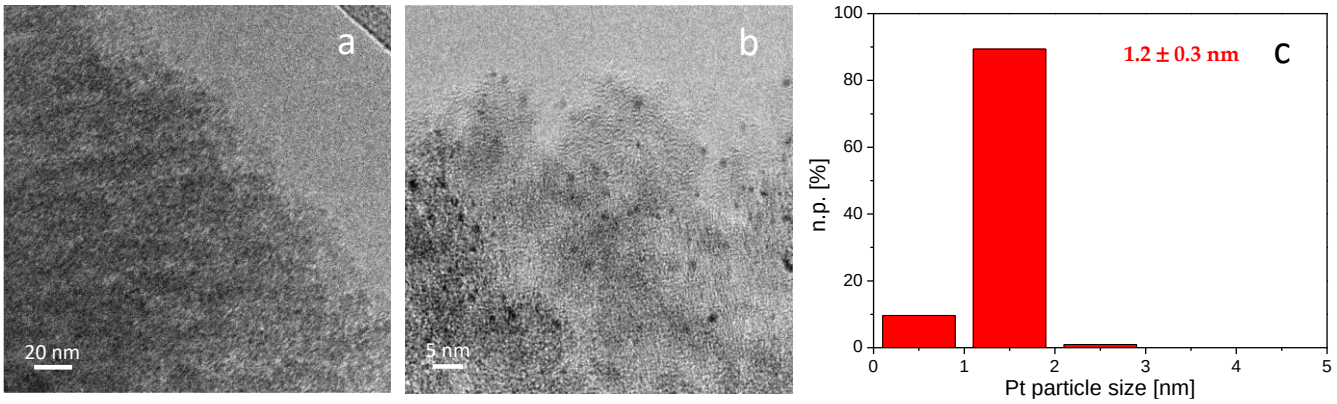

Figure 4. Representative TEM images of Pt-Mo(Na)_fresh (a) and Pt-Mo(Na)_400N (b). Pt particle size distribution of the sample treated at 400 °C in N_2(c). Instrumental magnification: 100000X and 250000X, respectively.

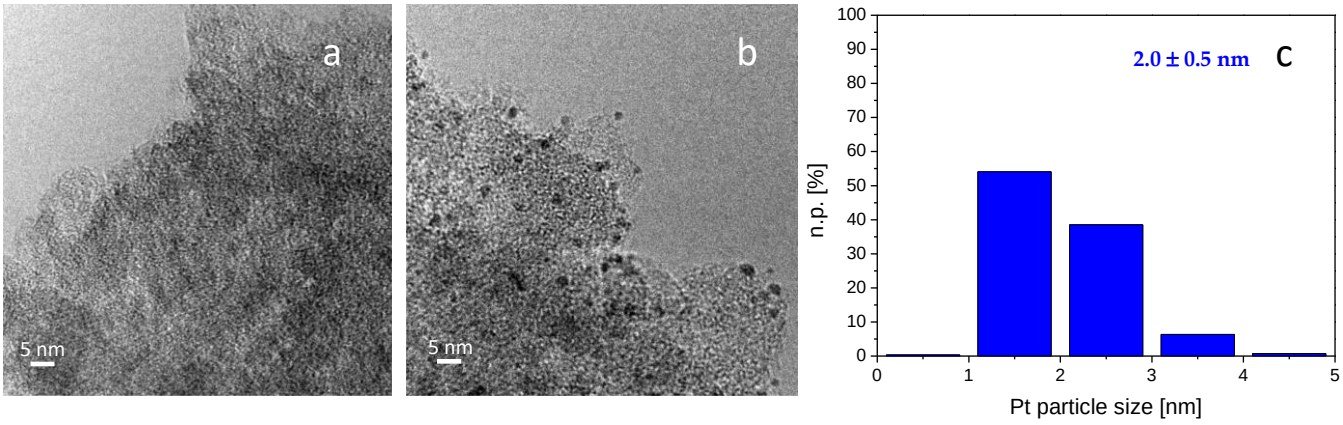

Figure 5. Representative TEM images collected on Pt-Mo(NH_4)_fresh (a) and Pt-Mo(NH_4)_400N (b). Particle size distribution of the sample treated at 400 °C in N_2 (c). Instrumental magnification: 100000X and 250000X, respectively.

It can be then concluded that a role of the Mo-precursor on the distribution of the Pt sites can be seen for Pt-Mo(Na)_400N and Pt-Mo(NH_4)_400N. Indeed, it was observed that the size of the Pt particles is larger and the particle size distribution is less homogeneous on the catalyst synthesized from $(NH_4)_6Mo_7O_{24}$ compared to that observed in the case of the one prepared using Na_2MoO_4 as precursor. These differences in terms of size and distribution of Pt NPs could be connected to the differences created by the thermal treatment on $(NH_4)_6Mo_7O_{24}$/C and the Na_2MoO_4/C, as different Mo species or Mo-C interaction. This could also lead to a different Pt-Mo/C interaction.

Therefore, the surface of each catalyst was investigated by XPS technique looking in particular at the Mo, Pt and C species. The XPS survey analyses showing binding energies (B.E.) (eV) and atomic % of Pt 4f and Mo 3d are reported in Table 3.

Table 3. XPS Survey analyses

			XPS line			
			C 1s	**O 1s**	**Pt 4f**	**Mo 3d**
n.	*Catalyst*					
1	Pt-Mo(Na)_fresh	*B.E. (eV)*	*284.6*	*532.7*	*73.7*	*nd*
		At. %	**88.9**	**9.7**	**0.01**	**0**
2	Pt-Mo(Na)_400N	*B.E. (eV)*	*284.6*	*532.7*	*71.9*	*231.9*
		At. %	**92.7**	**7.1**	**0.11**	**0.1**
3	Pt-Mo(NH_4)_fresh	*B.E. (eV)*	*284.6*	*532.6*	*73.7*	*232.9*
		At. %	**90.4**	**9.0**	**n.d.**	**0.13**
4	Pt-Mo(NH_4)_400N	*B.E. (eV)*	*284.6*	*532.5*	*71.9*	*232.5*
		At. %	**90.5**	**8.3**	**0.23**	**0.48**

The Pt-Mo(Na)_fresh (Table 3, entry 1) does not show any signal of Mo, in agreement with EDS results. In the other cases the B.E. resulted similar regardless the heating treatment and the Mo precursor. The Pt-Mo(Na)_400 showed a Mo atomic % of 0.07 (Table 3, entry 2). Otherwise, the Pt-Mo(NH_4)_fresh showed a Mo atomic % of 0.127 % (Table 3, entry 3), which increased up to 0.48 % in the Pt-Mo(NH_4)_400 (Table 3, entry 4). Considering the Pt 4f, we found that there is a shift in the B.E. between the fresh and the heat treated catalysts. Indeed, the B.E. shifted from 73.7 eV in the fresh (Table 3, entries 1 and 3) to 71.9 eV in the heat treated (Table 3, entries 2 and 4). Besides, we found that Pt NPs deposited on different Mo/C samples showed different surface exposure, which is always higher in the heat treated ones (see entries 2 and 4, Table 3). Moreover, looking at the XPS high-resolution spectra (Tables 4,5 and 6) some other interesting considerations can be done (images of the spectra are reported in the SI).

Table 4. High-resolution XPS analyses of Mo 3d region.

		Mo 3d	
Sample		Mo^{4+}	Mo^{6+}
Pt-Mo(Na)_fresh	*B.E. (eV)*	*nd*	*nd*
	At. %	-	-
Pt-Mo(Na)_400N	*B.E. (eV)*	*232.0*	*235.0*
	At. %	**44.2**	**55.8**
Pt-Mo(NH_4)_fresh	*B.E. (eV)*	*232.0*	*235.0*

	At. %	**55**	**44**
Pt-Mo(NH_4)_400N	*B.E. (eV)*	*232.7*	*235.8*
	At. %	**59**	**40**

Table 5. High-resolution XPS analyses of Pt 4f region.

		Pt 4f	
Sample		$Pt^{0/\delta+}$	$Pt^{II/IV}$
Pt-Mo(Na)_fresh	*B.E. (eV)*	*71.8*	*75.2*
	At. %	**46**	**53**
Pt-Mo(Na)_400N	*B.E. (eV)*	*72.2*	*73.4*
	At. %	**82.5**	**17.5**
Pt-Mo(NH_4)_fresh	*B.E. (eV)*	*nd*	*nd*
	At. %	**-**	**-**
Pt-Mo(NH_4)_400N	*B.E. (eV)*	*71.3*	*73.0*
	At. %	**78**	**22**

Table 6. High-resolution XPS analyses of C 1s region.

		C 1s			
sample		C-C/C=C	C-O	C=O	O-C=O
Pt-Mo(Na)_fresh	*B.E. (eV)*	*284.6*	*285.4*	*286.9*	*288.8*
	At. %	51.8	30.9	6.2	11.0
Pt-Mo(Na)_400N	*B.E. (eV)*	*284.6*	*285.3*	*286.3*	*288.0*
	At. %	32.1	43.8	13.8	6.8
Pt-Mo(NH_4)_fresh	*B.E. (eV)*	*284.6*	*285.8*	*287.5*	*289.6*
	At. %	65.6	23.2	5.3	5.9
Pt-Mo(NH_4)_400N	*B.E. (eV)*	*284.6*	*285.5*	*286.9*	*288.1*
	At. %	59.5	28.8	3.7	4.4

In Pt-Mo(Na)_fresh, no signal of Mo was revealed, while in the case of Pt-Mo(NH_4)_fresh, we found a distribution of Mo^{4+} (232 eV) and Mo^{6+} (235 eV) of 55% and 44 % respectively. Concerning the heat treated samples, the peak related to Mo 3d appeared in Pt-Mo(Na)_400.

From the deconvolution of the high-resolution spectrum we found 44.2% of Mo^{4+} (232 eV) and 55.8% of Mo^{6+} (see Table 4, line 2) [25], which was different for Pt-Mo(NH_4)_400N showing 59% of Mo^{4+} and 40% of Mo^{6+} (Table 4). Considering the deconvolution of the

high-resolution spectra of Pt 4f (Table 5), the peaks related to metallic Pt and PtO_x can be identified. As reported in literature, the standard reference B.E. value for Pt^0 is 71.0 eV [26], while slightly higher values can be attributed to the presence of partially oxidized Pt, indicated as $Pt^{\delta+}$. PtO and PtO_2 species show very similar binding energy values of 74.2 eV and 74.5 eV, respectively [27]. For this reason, it was rather difficult to discern between such two different oxidation states.

The deconvolution of the Pt-Mo(Na)_fresh spectrum showed two contributions of Pt: the first at 71.8 eV (46%) and the second at 75.2 eV (53%) (Table 5). We attributed the first to $Pt^{0/\delta+}$ while the second to $Pt^{II/IV}$. Comparing these data with the corresponding heat treated Pt-Mo(Na)_400N sample, it was found that the B.E. of $Pt^{0/\delta+}$ is not changing so much even if the percentage is double (from 46% to 82.5%at); differently, the B.E. of $Pt^{II/IV}$ decreased thus showing a higher contribution of Pt^{II} species than Pt^{IV}. Also the atomic % of oxidized species drastically decreased (from 53% to 17%). In the case of Pt-Mo(NH_4)_fresh the signal of Pt is very low and difficult to study. However, considering the Pt-Mo(NH_4)_400N, we found that the B.E. attributed to $Pt^{0/\delta+}$ was 71.3 eV lower than Pt-Mo(Na)_400N thus showing an higher contribution of Pt^0 in this sample. The B.E. of $Pt^{II/IV}$ was found at 73.0 eV slightly lower than Pt-Mo(Na)_400N meaning that the Pt^{II} specie slightly increases compared to Pt-Mo(Na)_400N.

Also a different support functionalization was found to depend on the Mo/C used. Investigating the high-resolution spectra of carbon (Table 6), we interestingly found that, upon heating, the C-O functionalization (285.4 eV) of the support always increased accompanied by a decrease of the amount of carboxylic groups (O-C=O at 288.0 eV). The C=O groups, on the contrary, showed a different behaviour, increasing in Pt-Mo(Na)_400N compared to Pt-Mo(Na)_fresh, while decreasing in Pt-Mo(NH_4)_400N compared to Pt-Mo(NH_4)_fresh.

On the basis of TEM and XPS analyses, we formulate a first hypothesis on the reason why fresh catalysts presented a negligible activity whilst the heat treated samples resulted active, and, most importantly, why the Pt-Mo(NH_4)_400N and Pt-Mo(Na)_400N behaved differently in terms of both activity and selectivity. Pt^0 has been reported as the active site for hydrogenation of cinnamaldehyde [28][29] and it is also reported that the reduction of CHO group is favoured by increasing particle size [29], even the activity decreased.

These data could explain the higher activity of the heat treated catalysts with respect to the fresh ones (see XPS data, Table 5), but also presented discrepancies. Indeed, Pt-Mo(Na)_400N and Pt-Mo(NH_4)_400N showed a similar $Pt^{0/\delta+}$ content (82% and 78%) and slightly different particle size (1.2 and 2.0 nm), which could be a consequence of the higher content of O-containing functionalities in the case of Pt-Mo(Na)_400N than Pt-Mo(NH_4)_400N (Table 6). However, Pt-Mo(NH_4)_400N showed a higher initial activity (Table 2) compared to Pt-Mo(Na)_400N, but it underwent to deactivation phenomena and presented a selectivity toward full hydrogenated product, i.e. HCOL.

We then considered the presence of different species of Mo, i.e. Mo^{IV} and Mo^{VI} as evidenced by XPS (Table 4). It was reported that the B.E. of Pt is reported to shift at lower value when Pt interacts with MoO_x [30]. Looking at the XPS data, we observed a lower B.E. for Pt in the case of Pt-Mo(NH_4)_400N (Table 5) (and a higher presence of MoO_2), thus confirming the higher reduction of Pt compared to Pt-Mo(Na)_400N. At the opposite, MoO_3 is reported to stabilize a more positive state of Pt [31] that can explain the high B.E. of Pt (72.2 eV, table 5) in Pt-Mo(Na)_400N.

Summarising, we can conclude that Mo-precursors direct the functionalisation of C during the calcination step and form different ratio of MoO_2 and MoO_3. These different

species have a different impact in the dispersion of Pt and in its final oxidation state which in turn modify the catalytic activity. However, even explaining the different activity, these findings cannot account for the different selectivity shown by the two catalysts. We thus search the explanation in a possible different acidity, as it is reported [32] that this parameter can have a decisive role in the hydrogenation rates of C=C/C=O.

Acid sites strength was investigated by NH_3-TPD analyses (Fig. 6). The quantification of the acid sites was very difficult because not all the profiles returned to the baseline level at high temperature. However, some qualitative considerations can be drawn.

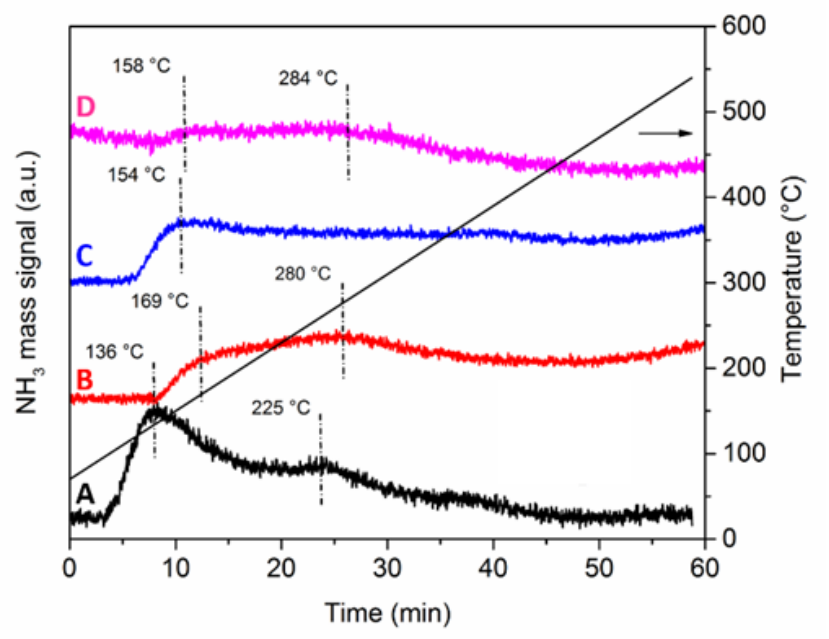

Figure 6. NH_3-TPD profiles of the Pt-Mo(NH_4)_fresh (A) and Pt-Mo(NH_4)_400N (B) samples, and of the Pt-Mo(Na)_fresh (C) and Pt-Mo(Na)_400N (D) samples.

Both Pt-Mo(NH_4)_fresh (sample A) and Pt-Mo(Na)_fresh (sample C), displayed desorption profiles with two main components, indicative of acid sites with different acid strength. The low-temperature component below 160 °C can be attributed to acid sites with low strength [33], while the broad feature at higher temperature can be due to highly dispersed Pt-Mo sites with medium acid strength [34].

The corresponding Pt-Mo(NH_4)_400N (sample B) and Pt-Mo(Na)_400N (sample D) have similar profiles, qualitatively less intense than the previous ones, but with both components at slightly higher desorption temperatures. Thus, the treatment in N_2 at 400 °C influenced the acidity of the samples. Moreover, there is a difference among the two thermal treated catalysts in the low-temperature region: the sample prepared from $(NH_4)_6Mo_7O_{24}$ shows a component at 169 °C whereas the one synthesized from Na_2MoO_4 is at 158 °C. Such difference in desorption temperature suggests that the Pt-Mo(NH_4)_400N catalyst has stronger acid sites compared to the Pt-Mo(Na)_400N sample.

It has been reported that a decrease in acidity results in greater electron density on the metal particles [35], which may cause a suppression in the C=C hydrogenation by enhancing the delocalisation of electrons in the adsorbed conjugated substrate.

Even if Pt usually activates the C=O group [17][36], a more acidic Pt catalyst has poorer electron density, which reduces the electron repulsion related to the C=C adsorption, favouring the formation of hydrocinnamaldehyde [37]. Thus, Pt-Mo(NH_4)_400N

mostly produced HCAL due to the presence of more acidic sites, resulting in a catalyst selective toward C=C hydrogenation.

5. Conclusions

Two different Mo precursors have been used to modify the active carbon used as support for Pt NPs. The thermal treatment of Mo/C before the Pt deposition resulted in an enhanced exposure of Pt, high NP dispersion and in higher reduction, thus promoting the catalytic activity. We ascribed this behaviour to the different functionalisation of carbon support which in turn affect MoO_2/MoO_3 ratio (XPS). However, the Pt-Mo(Na)_400N and Pt-Mo(NH_4)_400N samples behaved differently not only from an activity point of view, but also from that of selectivity. In particular, Pt-Mo(NH_4)_400N produced selectively HCAL, which subsequently underwent hydrogenation to HCOL. On the contrary, Pt-Mo(Na)_400N is able to hydrogenate C=C and C=O with almost comparable rate, which results in a 65:35 mol/mol ratio of HCAL:COL. Acidity studies revealed that another effect produced by the different Mo precursors is to vary the strength of acid sites on the surface, Pt-Mo(NH_4)_400N presenting stronger acid sites compared to Pt-Mo(Na)_400N. On the basis of the literature, we then ascribed the selectivity of Pt-Mo(NH_4)_400N toward C=C hydrogenation to the higher acidity of this catalyst respect to Pt-Mo(Na)_400N.

Supplementary Materials: The following are available online at www.mdpi.com/xxx/s1, Figure S1: EDS spectra of 1 wt% Pt-10 wt% Mo/C from Na_2MoO_4 before (a) and after (b) thermal treatment at 400 °C in N_2. Figure S2: TEM image collected on the Pt-Mo(NH_4)_400N sample and corresponding EDS map of the same region showing the relative location of Pt, Mo, C and O. Instrumental magnification: 20000×. Figure S3: XPS spectra. Figure S4: XRD spectrum.

Author Contributions: Conceptualization, M.S. and L.P.; methodology, M.S.; validation, M.S., L.P. and A.V.; formal analysis, M.M. and F.B.; investigation, M.S.; resources, L.P.; data curation, M.S., L.P. and M.M.; writing—original draft preparation, M.S.; writing—review and editing, M.S., A.V. and L.P.; supervision, L.P.; project administration, L.P.; All authors have read and agreed to the published version of the manuscript.

Funding: This research received no external funding.

Acknowledgments: The authors acknowledge support from the University of Milan through the APC initiative.

Conflicts of Interest: The authors declare no conflict of interest.

References

1. Taylor, M.J.; Jiang, L.; Reichert, J.; Papageorgiou, A.C.; Beaumont, S.K.; Wilson, K.; Lee, A.F.; Barth, J. V; Kyriakou, G. Catalytic Hydrogenation and Hydrodeoxygenation of Furfural over Pt(111): A Model System for the Rational Design and Operation of Practical Biomass Conversion Catalysts. **2017**.

2. Gorgas, N.; Stöger, B.; Veiros, L.F.; Kirchner, K. Highly Efficient and Selective Hydrogenation of Aldehydes: A Well-Defined Fe(II) Catalyst Exhibits Noble-Metal Activity. *ACS Catal.* **2016**, *6*, 2664–2672.

3. Zang, W.; Li, G.; Wang, L.; Zhang, X. Catalytic hydrogenation by noble-metal nanocrystals with well-defined facets: a review. *Catal. Sci. Technol.* **2015**, *5*, 2532–2553.

4. Kluson, P.; Cerveny, L. Selective hydrogenation over ruthenium catalysts. *Appl. Catal. A Gen.* **1995**, *128*, 13–31.

5. Quiroz, J.; Mai, E.F.; Da Silva, V.T. Synthesis of Nanostructured Molybdenum Carbide as Catalyst for the

Hydrogenation of Levulinic Acid to γ-Valerolactone. *Top. Catal.* **2016**, *59*, 148–158. 406

6. Hoang-Van, C.; Zegaoui, O. Studies of high surface area Pt/MoO3 and Pt/WO3 catalysts for selective hydrogenation reactions. II. Reactions of acrolein and allyl alcohol. *Appl. Catal. A Gen.* **1997**, *164*, 91–103. 407 408

7. He, Z.; Hu, M.; Wang, X. Highly effective hydrodeoxygenation of guaiacol on Pt/TiO2: Promoter effects. *Catal. Today* **2018**, *302*, 136–145. 409 410

8. Force, C.; Belzunegui, J..; Sanz, J.; Martínez-Arias, A.; Soria, J. Influence of Precursor Salt on Metal Particle Formation in Rh/CeO2 Catalysts. *J. Catal.* **2001**, *197*, 192–199. 411 412

9. REN, S.; QIU, J.; WANG, C.; XU, B.; FAN, Y.; CHEN, Y. Influence of Nickel Salt Precursors on the Hydrogenation Activity of Ni/γ-Al2O3 Catalyst. *Chinese J. Catal.* **2007**, *28*, 651–656. 413 414

10. GALLEZOT, P.; RICHARD, D. Selective Hydrogenation of α,β-Unsaturated Aldehydes. *Catal. Rev.* **1998**, *40*, 81–126. 415 416

11. Mäki-Arvela, P.; Hájek, J.; Salmi, T.; Murzin, D.Y. Chemoselective hydrogenation of carbonyl compounds over heterogeneous catalysts. *Appl. Catal. A Gen.* **2005**, *292*, 1–49. 417 418

12. Eilerman, R.G.; Staff, U. by Cinnamic Acid, Cinnamaldehyde, and Cinnamyl Alcohol. *Kirk-Othmer Encycl. Chem. Technol.* 2014, 1–11. 419 420

13. Gottardi, M.; Grün, P.; Bode, H.B.; Hoffmann, T.; Schwab, W.; Oreb, M.; Boles, E. Optimisation of trans-cinnamic acid and hydrocinnamyl alcohol production with recombinant Saccharomyces cerevisiae and identification of cinnamyl methyl ketone as a by-product. *FEMS Yeast Res.* **2017**, *17*, 1–10. 421 422 423

14. Ma, H.; Wang, L.; Chen, L.; Dong, C.; Yu, W.; Huang, T.; Zhou, Y. Pt nanoparticles deposited over carbon nanotubes for selective hydrogenation of cinnamaldehyde. *Catal. Commun.* **2007**, *8*, 452–456. 424 425

15. Asedegbega-Nieto, E.; Bachiller-Baeza, B.; Guerrero-Ruíz, A.; Rodríguez-Ramos, I. Modification of catalytic properties over carbon supported Ru-Cu and Ni-Cu bimetallics: I. Functional selectivities in citral and cinnamaldehyde hydrogenation. *Appl. Catal. A Gen.* **2006**, *300*, 120–129. 426 427 428

16. Leng, F.; Gerber, I.C.; Axet, M.R.; Serp, P. Selectivity shifts in hydrogenation of cinnamaldehyde on electron-deficient ruthenium nanoparticles. *Comptes Rendus Chim.* **2018**, *21*, 346–353. 429 430

17. Giroir-Fendler, A.; Richard, D.; Gallezot, P. Selectivity in Cinnamaldehyde Hydrogenation of Group-VIII Metals Supported on Graphite and Carbon. In *Heterogeneous Catalysis and Fine Chemicals*; Guisnet, M., Barrault, J., Bouchoule, C., Duprez, D., Montassier, C., Pérot, G.B.T.-S. in S.S. and C., Eds.; Elsevier, 1988; Vol. 41, pp. 171–178 ISBN 0167-2991. 431 432 433 434

18. Delbecq, F.; Sautet, P. Competitive C⊚C and C⊚O Adsorption of α-β-Unsaturated Aldehydes on Pt and Pd Surfaces in Relation with the Selectivity of Hydrogenation Reactions: A Theoretical Approach. *J. Catal.* **1995**, *152*, 217–236. 435 436 437

19. Hao, C.H.; Guo, X.N.; Pan, Y.T.; Chen, S.; Jiao, Z.F.; Yang, H.; Guo, X.Y. Visible-Light-Driven Selective Photocatalytic Hydrogenation of Cinnamaldehyde over Au/SiC Catalysts. *J. Am. Chem. Soc.* **2016**, *138*, 9361–9364.

20. Mahata, N.; Gonçalves, F.; Pereira, M.F.R.; Figueiredo, J.L. Selective hydrogenation of cinnamaldehyde to cinnamyl alcohol over mesoporous carbon supported Fe and Zn promoted Pt catalyst. *Appl. Catal. A Gen.* **2008**, *339*, 159–168.

21. Wang, D.; Zhu, Y. An Effective Pt-Cu/SiO2 Catalyst for the Selective Hydrogenation of Cinnamaldehyde. *J. Chem.* **2018**, *2018*.

22. Wang, D.; Zhu, Y.; Tian, C.; Wang, L.; Zhou, W.; Dong, Y.; Han, Q.; Liu, Y.; Yuan, F.; Fu, H. Synergistic effect of Mo2N and Pt for promoted selective hydrogenation of cinnamaldehyde over Pt–Mo2N/SBA-15. *Catal. Sci. Technol.* **2016**, *6*, 2403–2412.

23. Shu, Y.; Chen, T.; Chan, H.C.; Xie, L.; Gao, Q. Chemoselective Hydrogenation of Cinnamaldehyde on Iron-Oxide Modified Pt/MoO3−y Catalysts. *Chem. - An Asian J.* **2018**, *13*, 3737–3744.

24. Dal Santo, V.; Dossi, C.; Fusi, A.; Psaro, R.; Mondelli, C.; Recchia, S. Fast transient infrared studies in material science: development of a novel low dead-volume, high temperature DRIFTS cell. *Talanta* **2005**, *66*, 674–682.

25. Wu, H.; Lian, K. The Development of Pseudocapacitive Molybdenum Oxynitride Electrodes for Supercapacitors. *ECS Trans.* **2014**, *58*, 67–75.

26. Briggs, D. X-ray photoelectron spectroscopy (XPS). *Handb. Adhes. Second Ed.* **2005**, 621–622.

27. Mazzotta, E.; Rella, S.; Turco, A.; Malitesta, C. XPS in development of chemical sensors. *RSC Adv.* **2015**, *5*.

28. Reyes, P.; Rodríguez, C.; Pecchi, G.; Fierro, J.L.G. Promoting effect of Mo on the selective hydrogenation of cinnamaldehyde on Rh/SiO2 catalysts. *Catal. Letters* **2000**, *69*, 27–32.

29. Durndell, L.J.; Parlett, C.M.A.; Hondow, N.S.; Isaacs, M.A.; Wilson, K.; Lee, A.F. Selectivity control in Pt-catalyzed cinnamaldehyde hydrogenation. *Sci. Rep.* **2015**, *5*, 9425.

30. Wang, A.-L.; Liang, C.-L.; Lu, X.-F.; Tong, Y.-X.; Li, G.-R. Pt–MoO3–RGO ternary hybrid hollow nanorod arrays as high-performance catalysts for methanol electrooxidation. *J. Mater. Chem. A* **2016**, *4*, 1923–1930.

31. Jackson, S.D.; Willis, J.; McLellan, G.D.; Webb, G.; Keegan, M.B.T.; Moyes, R.B.; Simpson, S.; Wells, P.B.; Whyman, R. Supported metal catalysts: Preparation, characterization, and function. i. Preparation and physical characterization of platinum catalysts. *J. Catal.* 1993, *139*, 191–206.

32. Lashdaf, M.; Nieminen, V.V.; Tiitta, M.; Venäläinen, T.; Österholm, H.; Krause, O. Role of acidity in hydrogenation of cinnamaldehyde on platinum beta zeolite. *Microporous Mesoporous Mater.* **2004**, *75*, 149–158.

33. Boufaden, N.; Akkari, R.; Pawelec, B.; Fierro, J.L.G.; Zina, M.S.; Ghorbel, A. Dehydrogenation of methylcyclohexane to toluene over partially reduced silica-supported Pt-Mo catalysts. *J. Mol. Catal. A Chem.* **2016**, *420*, 96–106.

34. He, Z.; Hu, M.; Wang, X. Highly effective hydrodeoxygenation of guaiacol on Pt/TiO2: Promoter effects. *Catal. Today* **2018**, *302*, 136–145.

35. Gallezot, P. The State and Catalytic Properties of Platinum and Palladium in Faujasite-type Zeolites. *Catal. Rev.* **1979**, *20*, 121–154.

36. Delbecq, F.; Sautet, P. Competitive C=C and C=O Adsorption of α-β unsaturated aldehydes on Pt and Pd surfaces in relation with the selectivity of hydrogenation reactions: A theoretical approach. *J. Catal.* 1995, *152*, 217–236.

37. Lashdaf, M.; Nieminen, V.-V.; Tiitta, M.; Venäläinen, T.; Österholm, H.; Krause, O. Role of acidity in hydrogenation of cinnamaldehyde on platinum beta zeolite. *Microporous Mesoporous Mater.* **2004**, *75*, 149–158.